ELSEVIER

Journal of Alloys and Compounds 321 (2001) 84–90

Journal of ALLOYS AND COMPOUNDS

www.elsevier.com/locate/jallcom

Thermodynamic modeling of the miscibility gaps and the metastability in the R_2O_3–SiO_2 systems (R=La, Sm, Dy, and Er)

Sung S. Kim[a,*], Jun Y. Park[a], Thomas H. Sanders Jr.[b]

[a]*School of Materials Science and Engineering, Hong Ik University, Jochiwon 339-701, South Korea*
[b]*School of Materials Science and Engineering, Georgia Institute of Technology, Atlanta, GA 30332-0245, USA*

Received 18 November 2000; accepted 8 February 2001

Abstract

A range of compositions and temperatures below the monotectic temperature exists where there are thermodynamic restrictions that prevent the equilibrium solid from forming directly from the undercooled homogeneous liquid. In this region the solid can form only after liquid–liquid phase separation has occurred. As suggested by earlier research, the thermodynamic restrictions on the crystallization process may be useful to control the crystallized grain structure in glass–ceramic systems. Thus, understanding the thermodynamic limitations on the formation of the solid in monotectic systems could have commercial significance. In the present paper, the metastable liquidus boundaries, liquid miscibility gaps, and spinodal curves in the binary La_2O_3–SiO_2, Sm_2O_3–SiO_2, Dy_2O_3–SiO_2, and Er_2O_3–SiO_2 systems were calculated using analytical expressions for the Gibbs free energies of the liquid phases.

Keywords: Thermodynamic properties; Monotectic; Liquidus; Silicates; Amorphous materials; Liquid quenching; Thermodynamic properties

1. Introduction

Silicate glasses containing rare earth oxides have been studied from the viewpoint of color and fluorescence indicators for many decades [1]. Glasses containing rare earth oxides as dopants have been used as lasers, sensors, optical amplifiers, and radiation resistant glasses. Glasses containing rare earth oxides as major components have been developed for the production of optical rotators based on the Faraday effect [2]. Recently, various glasses with the rare earth oxide were prepared and converted to glass–ceramics by heat treatment [3–5]. The effects of rare earth ions on the physical properties of glass–ceramics were investigated. The physical properties of glass–ceramics are closely related with their microstructure. Therefore, in order to optimize the microstructure of the glass–ceramics, the crystallization process of the glasses should be controlled and the phases and phase relationships of the relevant multi-component system should be investigated closely during the heat treatment.

Phase diagrams for the binary rare earth silicate systems show a broad range of liquid immiscibility. Therefore, it is not possible to produce homogeneous glasses containing modest amounts of rare earth oxide due to the occurrence of immiscibility. Since the 2-liquid regions for compositions containing greater quantities of rare earth oxides are located in extremely high temperature, few investigations on the glass-forming behavior of these systems have been performed. Toropov and coworkers [6–8] determined phase diagrams in several rare earth silicate systems experimentally. In the La_2O_3–SiO_2 system [6], a range of liquid miscibility gap was found between 2.3 and 23.0 mol% La_2O_3 at monotectic temperature 1675°C and the critical point is located at 7.6 mol% La_2O_3 and 2075°C. In the Sm_2O_3–SiO_2 system [7], a region of liquid immiscibility was found between 2.2 and 24.2 mol% Sm_2O_3 at monotectic temperature 1700°C and the critical point is located at 8.1 mol% Sm_2O_3 and 2190°C. In the Dy_2O_3–SiO_2 system [8], a range of liquid miscibility gap was found between 1.3 and 22.0 mol% Dy_2O_3 at monotectic temperature 1675°C and the critical point is located at 8.0 mol% Dy_2O_3 and 2320°C. In the Er_2O_3–SiO_2 system [8], a region of liquid immiscibility was found between 1.4 and 22.7 mol% Er_2O_3 at monotectic temperature 1700°C and the critical point is located at 11.4 mol% Er_2O_3 and 2259°C. Since the location of the critical points in these

*Corresponding author. Tel.: +82-41-860-2580; fax: +82-41-862-2774.

E-mail address: sungkim@wow.hongik.ac.kr (S.S. Kim).

0925-8388/01/$ – see front matter
PII: S0925-8388(01)00974-4

systems was not clear, Hageman and Oonk [9] investigated the region of the miscibility gap in the La_2O_3–SiO_2 system. Due to few researches on the rare earth silicate systems, it is valuable to perform the basic theoretical studies on the glasses and the glass–ceramics containing the rare-earth oxides.

Cahn [10] suggested the mechanism of liquid immiscibility in a single-phase liquid by schematically describing the Gibbs free energy of a liquid phase in a hypothetical binary monotectic system as a function of temperature. Using the concept of the metastable liquidus he demonstrated that under certain conditions an equilibrium phase is unstable in the presence of the metastable homogeneous liquid phase. Fig. 1 shows a monotectic phase diagram with a solid that is a line compound. In region I, bounded by the metastable liquidus and the spinodal curve below the monotectic temperature, the nucleation of the stable solid phase from the single-phase liquid is retarded until the liquid separates into two liquids. This can be explained by considering the behavior of Gibbs free-energy curves for the liquid and solid at temperature T_4 in Fig. 2. Any tangent line to the homogeneous liquid free energy curve in region I, being located below the free energy of the solid phase at its stable composition, shows a negative driving force for the formation of solid. In region II, bounded by the metastable liquidus and the spinodal curve above the monotectic temperature, it is possible to nucleate and grow a solid phase before liquid–liquid separation occurs. The solid remains metastable in this region until the liquid separates into two liquids, into which it will dissolve. This can also be illustrated by considering the behavior of Gibbs free energy curves of the liquid and solid at T_2 in Fig. 2. Any tangent line to the homogeneous liquid free energy curve in region II, being located above the free energy of the solid phase at its stable composition, shows a positive driving force for the formation of the solid. Therefore, there exist some composition and temperature ranges where a stable solid cannot form directly from an undercooled liquid phase under the monotectic temperature and a metastable solid cannot dissolve into a single phase liquid above the monotectic temperature.

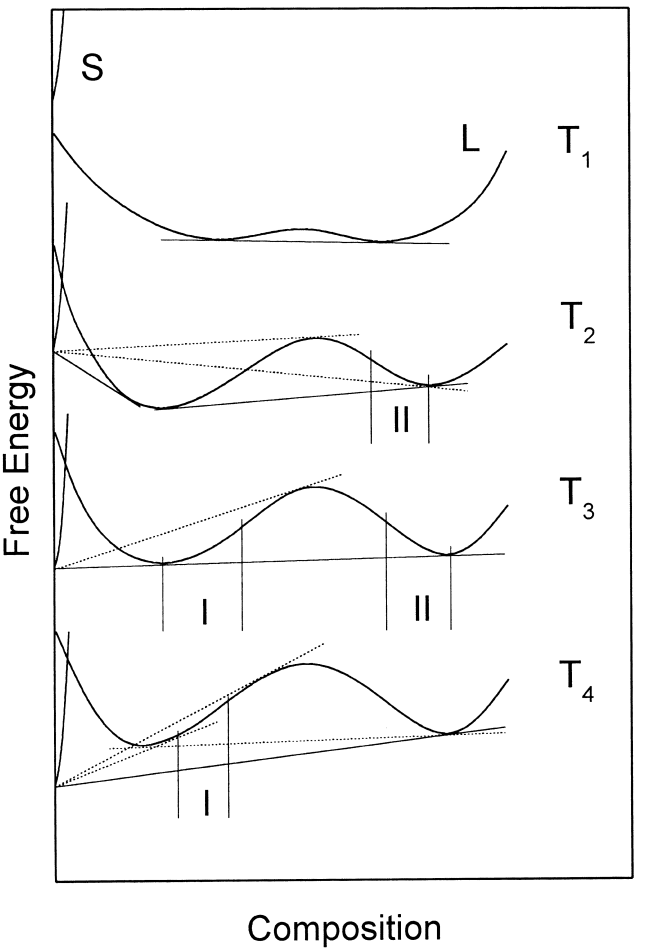

Fig. 2. Free energy curves vs. composition near the monotectic temperature. The stable and metastable liquidus compositions are shown by drawing tangent lines. Temperatures correspond to those of Fig. 1 (L: liquid phase, S: solid phase).

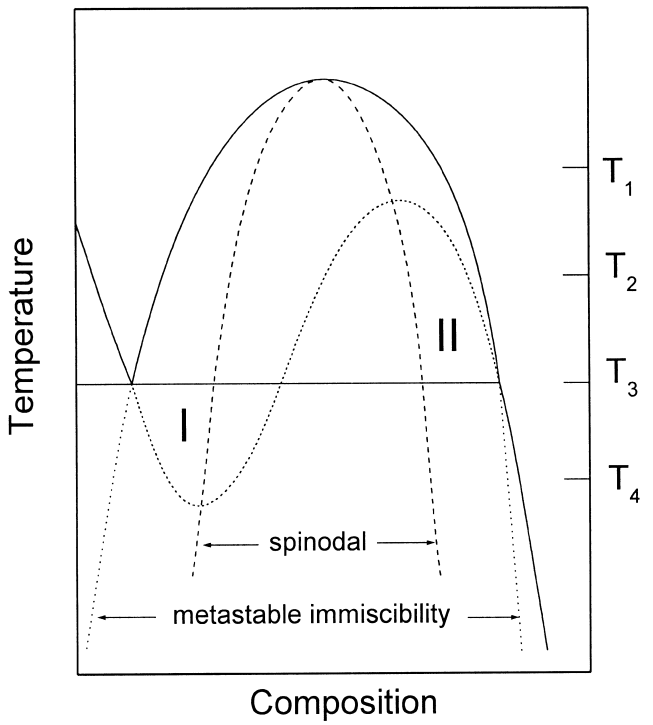

Fig. 1. Phase diagram showing the metastable liquidus through the miscibility gap.

Computer modeling of thermodynamic properties of phases makes it possible to extract information from existing phase diagrams without the need for additional experiments. Furthermore, extensions of equilibrium data to metastable data and vice versa can be made. Once the Gibbs free-energy expressions for liquid phases are determined, regions I and II can be calculated. By using the Gibbs free-energy expressions for the liquid phases, it becomes possible to extend the work of Cahn [10] and

identify compositions and temperatures to verify the influence of phase separation on the crystallization process experimentally. Hageman and Oonk [9] developed a thermodynamic model for the liquid phase to calculate the critical point of the miscibility gap after investigating the miscibility gap in several silicate systems including the La_2O_3–SiO_2 system. However, there is a flaw in their approach. When calculating the equilibrium compositions at the monotectic temperature, they considered only equilibrium between two liquids and did not include the solid phase in their calculations. Therefore, their result cannot be used to calculate the monotectic temperature and composition precisely. Recently, Wang and coworkers [11,12] assessed thermodynamically the binary phase diagrams of the Nd_2O_3–SiO_2, Sm_2O_3–SiO_2, and Gd_2O_3–SiO_2 systems by using the experimental data in the literatures, and they used the second-order Redlich–Kister equation [13] to express the Gibbs free energy of the liquid phases as a function of composition and temperature. The phase diagrams were calculated through the whole composition but the large difference between the calculated and experimental results exists near the top of miscibility gaps.

Recently Kim and Sanders [14] assessed the metastable liquidi as well as the miscibility gaps in alkaline-earth silicate systems in order to estimate thermodynamic restrictions near the monotectic. In the present work, the first-order Redlich–Kister solution model was used to describe the thermodynamic properties of liquid solutions in the high silica regions of the binary La_2O_3–SiO_2, Sm_2O_3–SiO_2, Dy_2O_3–SiO_2, and Er_2O_3–SiO_2 systems. The multiple linear regression method was used to determine the interaction parameters of liquid solutions from miscibility gap data in the literature. The miscibility gaps calculated in the present work were compared and discussed with other data available from the literature. By calculating the spinodals and metastable liquidi, regions I and II in Fig. 1 were determined and Cahn's suggestion was discussed for the above systems. The results of the calculation will provide direction for future experiments designed to investigate liquid–liquid phase separation.

2. Thermodynamic methodology

In binary systems with asymmetric miscibility gaps, the Gibbs free energy of the phase cannot be expressed using a regular solution model. Instead, a subregular solution model can be applied to account for the asymmetry. In the present work, a solution model was chosen in the form of the Redlich–Kister equation, which proved to have the best fitting capability among several solution models [15]. When the standard states are solid phases (s) of pure components i and j, the Gibbs free energies of liquid (l) and the solid (s) phases in the i–j system are given by

$$G_m^l = (1-x)\Delta G_i^{s\to l} + x\Delta G_j^{s\to l} + RT[(1-x)\ln(1-x) + x\ln x] + x(1-x)[A^0 + A^1(1-2x)] \quad (1)$$

where x is the mole fraction of component j, $\Delta G_i^{s\to l}$ and $\Delta G_j^{s\to l}$ are the differences in Gibbs free energy between the s phase and the l phase of pure components i and j, respectively, and A^0 and A^1 are the interaction parameters of the liquid phase. In this work, the interaction parameters are expressed as linear functions of temperature.

The partial molar Gibbs free energies of components i and j for the liquid phase (l) are given by

$$G_i^{-l} = \Delta G_i^{s\to l} + RT\ln(1-x) + x^2[A^0 + A^1(3-4x)] \quad (2a)$$

$$G_j^{-l} = \Delta G_j^{s\to l} + RT\ln x + (1-x)^2[A^0 + A^1(1-4x)] \quad (2b)$$

To model phase diagrams, basic physical data such as heat capacity, melting point, and heat of fusion are required. The heat capacity data, however, are available for only a few oxides and are sometimes inaccurate. In the present calculation, only the melting points and heats of fusion of components were used to calculate the interaction parameters of the solid and liquid phases. If the small heat capacity corrections to the enthalpy and entropy of fusion are neglected, then

$$\Delta G_i^{s\to l} = (\Delta H_{f,i})\left(1 - \frac{T}{T_{m,i}}\right) \quad (3a)$$

$$\Delta G_j^{s\to l} = (\Delta H_{f,j})\left(1 - \frac{T}{T_{m,j}}\right) \quad (3b)$$

where $T_{m,i}$, $T_{m,j}$, $\Delta H_{f,i}$, and $\Delta H_{f,j}$ are the melting points and the enthalpies of fusion of the component i and j, respectively. The frequently cited melting point and heat of fusion of silica [16,17] were used in the present calculations. For the rare earth oxides, the constant entropy of fusion of 6 cal/mol·K [18] was applied, which was obtained from using the limiting slopes of the liquidus curves at 100% R_2O_3 in the binary R_2O_3–Al_2O_3 systems (from R = La to Dy).

To obtain the interaction parameters of the liquid phase, three equilibrium conditions were considered. First, at the top of the liquid miscibility gap, the second and third derivatives of the Gibbs free energy function, with respect to composition, must be zero, i.e.

$$\left(\frac{\partial^2 G_m^l}{\partial x^2}\right) = RT_c\left[\frac{1}{(1-x_c)} + \frac{1}{x_c}\right] - 2A^0 - 6A^1(1-2x_c) = 0 \quad (4a)$$

$$\left(\frac{\partial^3 G_m^l}{\partial x^3}\right) = RT_c\left[\frac{1}{(1-x_c)^2} - \frac{1}{x_c^2}\right] + 12A^1 = 0 \quad (4b)$$

where T_c and x_c are the temperature and composition at the

critical point, respectively. Rearranging the above-described equations gives

$$RT_c\left[\frac{1}{(1-x_c)}+\frac{1}{x_c}\right]=2A^0+6A^1(1-2x_c) \quad (5a)$$

$$RT_c\left[\frac{1}{(1-x_c)^2}-\frac{1}{x_c^2}\right]=-12A^1 \quad (5b)$$

Second, below the critical point of the miscibility gap, the equilibrium condition for the coexistence of two liquid phases requires equality of the partial molar Gibbs free energies of each component. Therefore, using Eqs. (2a) and (2b) the following equations for i and j components must be satisfied:

$$RT\ln(1-x_1)+x_1^2[A^0+A^1(3-4x_1)] = RT\ln(1-x_2)+x_2^2[A^0+A^1(3-4x_2)] \quad (6a)$$

$$RT\ln x_1+(1-x_1)^2[A^0+A^1(1-4x_1)] = RT\ln x_2+(1-x_2)^2[A^0+A^1(1-4x_2)] \quad (6b)$$

where the x_1 and x_2 are two equilibrium compositions of l_1 and l_2 phases on the liquid miscibility gap at temperature T. Rearranging the above-described equations gives

$$RT\ln[(1-x_1)/(1-x_2)] = A^0(x_2^2-x_2^2)+A^1[x_2^2(3-4x_2)-x_2^2(3-4x_1)] \quad (7a)$$

$$RT\ln(x_1/x_2) = A^0[(1-x_2)^2-(1-x_1)^2] + A^1[(1-x_2)^2(1-4x_2)-(1-x_1)^2(1-4x_1)]. \quad (7b)$$

Third, at the monotectic temperature (T_{mo}), equilibrium between two liquids and pure solid for component i is required. Therefore, Eq. (2a) must be zero at compositions x_1 and x_2 since in the standard state of the pure solid there is no solubility of component j in component i.

$$\Delta H_{f,i}(1-T_{mo}/T_{m,i})+RT_{mo}\ln(1-x_{mo}) + x_{mo}^2[A^0+A^1(3-4x_{mo})]=0 \quad (8)$$

where x_{mo}'s are two equilibrium compositions x_1 and x_2 of l_1 and l_2 phases on the liquid miscibility gap at T_{mo}, respectively. Rearranging the above-described equation gives

$$-[\Delta H_{f,i}(1-T_{mo}/T_{m,i})+RT_{mo}\ln(1-x_{mo})]/x_{mo} = A^0x_{mo}+A^1x_{mo}(3-4x_{mo}) \quad (9)$$

The above-given expressions (Eqs. (5a), (5b), (7a), (7b), and (9)) can be considered as a linear combination, i.e.

$$Y=A^0X_1+A^1X_2. \quad (10a)$$

When interaction parameters are given by a linear function of temperature, the above-described equation can be expressed as

$$Y=A_1^0X_1+A_2^0TX_1+A_1^1X_2+A_2^1TX_2 \quad (10b)$$

where, $A^0=A_1^0+A_2^0T$ and $A^1=A_1^1+A_2^1T$.

Using experimental liquid miscibility data, the interaction parameters in Eqs. (10a) and (10b) can be determined through a multiple linear regression method [14,19], which permits the metastable liquidus, as well as the equilibrium miscibility gap, to be calculated as a function of temperature.

Either stable or metastable liquidus compositions can be determined by extrapolating the tangent to the free energy curve of the liquid phase to the bottom of the free energy curve of the pure solid phase at the composition of the pure solid phase, as shown in Fig. 2. This condition can be obtained by substituting x_l for x_{mo} and T for T_{mo} in Eq. (8) respectively, where x_l refers to the stable or metastable liquidus composition at the temperature T. By solving Eq. (8) in this manner about the monotectic temperature, the metastable liquidi inside the miscibility gap and the stable liquidi outside the miscibility gap can be obtained. The spinodal curve was calculated by applying the condition that the second derivative of free energy must be zero, i.e.

$$\left(\frac{\partial^2 G_m^l}{\partial x^2}\right)=RT\left[\frac{1}{(1-x)}+\frac{1}{x}\right]-2A^0-6A^1(1-2x)=0 \quad (11)$$

The above-described equation can be solved numerically.

3. Results and discussion

The calculated miscibility gaps in the La_2O_3–SiO_2, Sm_2O_3–SiO_2, Dy_2O_3–SiO_2, and Er_2O_3–SiO_2 systems are shown in Figs. 3–6. In these figures, the solid, dot, and dashed curves show the miscibility gaps, metastable liquidus curves and spinodal curves calculated in the present work, respectively. Also shown are the stable liquidus and the metastable extensions of the miscibility gap. The circle symbols represent the experimental data by Toropov and co-workers [6–8], which were used to determine the interaction parameters of the liquid solutions in the present work. The liquid immiscibility in many oxide systems is related to differences in ionic field strength Z/a^2, where Z = the cation charge and a = the distance between the cation and the oxygen ion [20,21]. However, since the lanthanide ions all have similar electronic configurations and exhibit a small difference in ionic radii (from 1.06 Å for La^{3+} to 0.88 Å for Er^{3+}) with R^{3+} being the common oxidation state, the cationic field strength within the lanthanide group is very similar. Therefore, miscibility gaps in the present rare earth silicate systems show a similar size.

Table 1 summarizes the interaction parameters of the

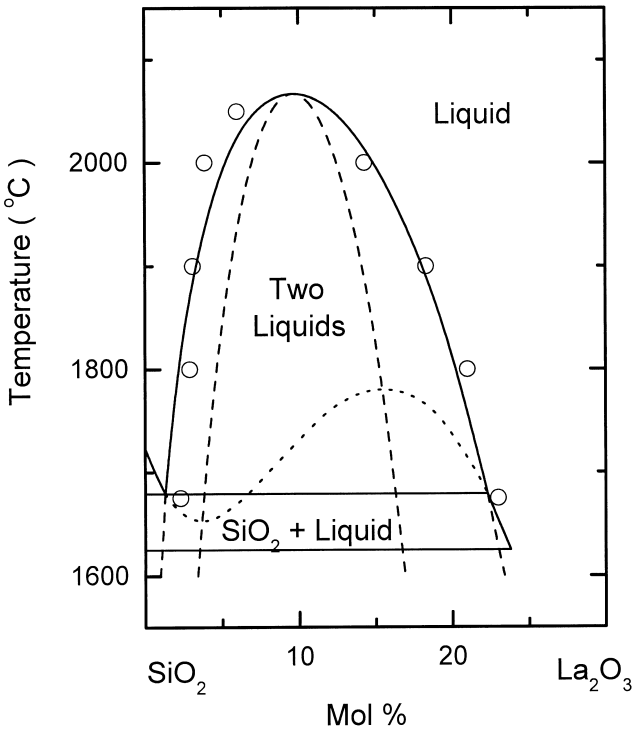

Fig. 3. Calculated phase diagram and metastable liquidus in the La_2O_3–SiO_2 system (○: experimental data [6]).

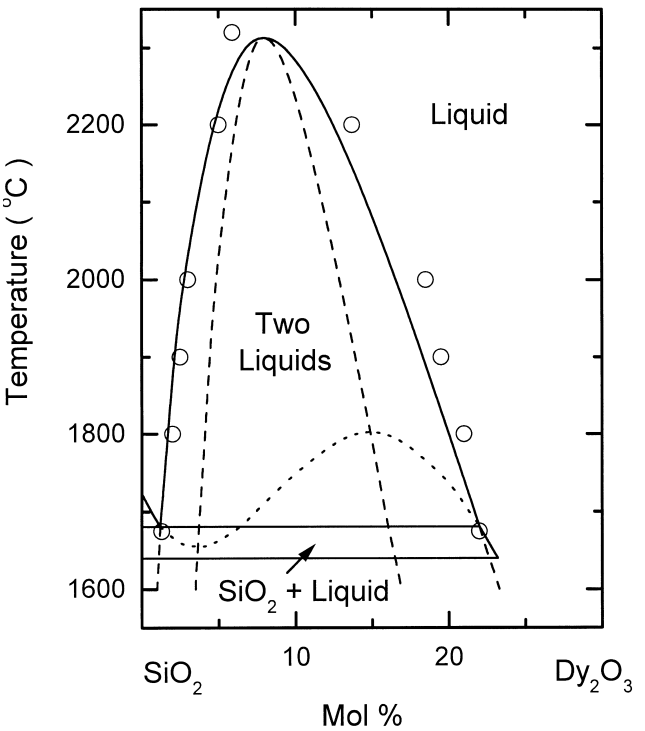

Fig. 5. Calculated phase diagram and metastable liquidus in the Dy_2O_3–SiO_2 system (○: experimental data [8]).

liquid solutions in the present systems. The calculated miscibility gaps in Figs. 3–6 agree well with the experimental data through the whole region. Hageman and Oonk [9] tried to fit their experimental data to their own solution model and obtained good results for the several silicate systems. However, it should be mentioned that they

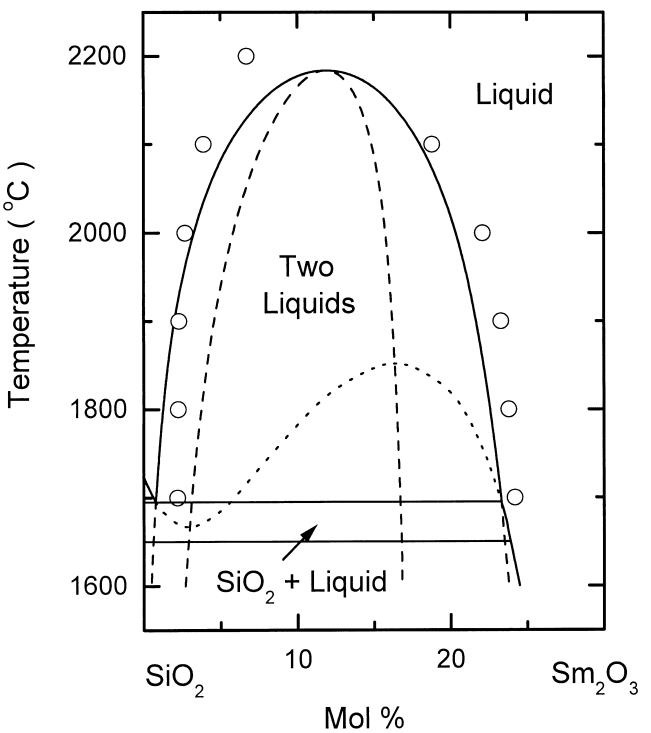

Fig. 4. Calculated phase diagram and metastable liquidus in the Sm_2O_3–SiO_2 system (○: experimental data [7]).

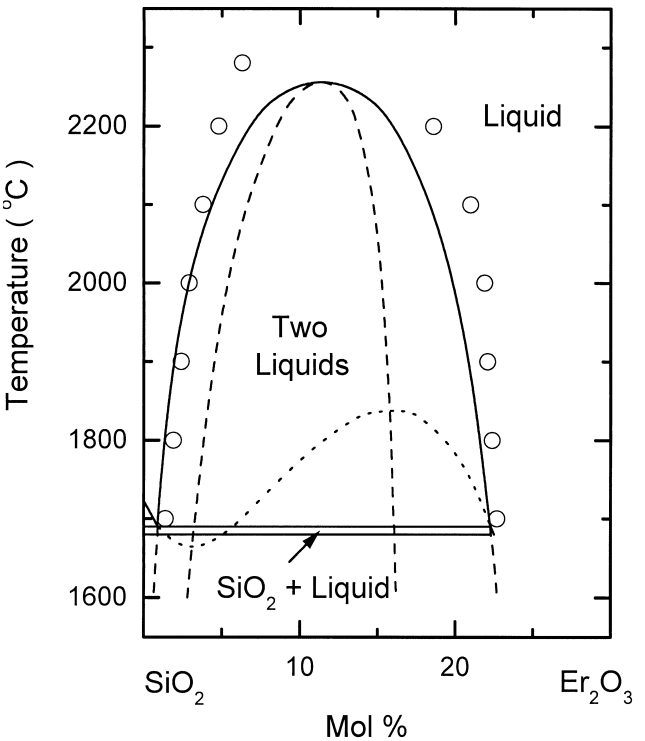

Fig. 6. Calculated phase diagram and metastable liquidus in the Er_2O_3–SiO_2 system (○: experimental data [8]).

Table 1
Calculated interaction parameters of liquid phases in the rare earth silicate systems (in kJ/mol). Excess free energy: $G^E = x(1-x)[A^0 + A^1(1-2x)]$, $x = x_{R_2O_3}$

Systems		Interaction parameters
La_2O_3–SiO_2	A^0	$-39.8971 + 0.0094T$/K
	A^1	$23.9518 - 0.0060T$/K
Sm_2O_3–SiO_2	A^0	$-93.9203 + 0.0341T$/K
	A^1	$48.2483 - 0.0168T$/K
Dy_2O_3–SiO_2	A^0	$2.7314 - 0.0133T$/K
	A^1	$4.5486 + 0.0044T$/K
Er_2O_3–SiO_2	A^0	$-81.0908 + 0.0274T$/K
	A^1	$40.9276 - 0.0132T$/K

did not consider the equilibria between two liquid phases and a SiO_2 phase at the T_{mono}. Therefore, it is doubtful whether their method could be applied to various systems. For the Sm_2O_3–SiO_2 system, the present calculation from the first-order Redlich–Kister model shows good agreement with the experimental data [7] and the result calculated from the second-order Redlich–Kister model [11]. The results of the present calculations are summarized in Table 2 and compared with experimental data in the literature.

The stability of the liquidus is dependent only on its location, with respect to the miscibility gap; thus, it is a single continuous curve throughout the composition range. Therefore, as suggested by Cahn [10], the metastable liquidus might be obtained from the extrapolation of the stable liquidus. However, it is very difficult to extrapolate the short stable liquidus into the miscibility gap. Furthermore, it is impossible to estimate the minimum and maximum points on the metastable liquidus. As the melting point of solid phase increases, compared to T_{mono}, and the location of the solid phase is closer to the miscibility gap, the height of metastable liquidus near T_{mono} is expected to be greater. Figs. 3–6 clearly show that the shape of the metastable liquidus is dependent on both the melting point and the location of SiO_2, relative to the miscibility gap. In the present silicate systems, the size of region I is smaller than that of region II and the metastable liquidi at T_{mono} pass approximately through a position 1/4–1/5 the size of the miscibility gaps. This result is similar to that of the alkaline earth silicate systems [14].

Table 3 shows the results of an analysis on the regions where a metastable solid can exist. Δx_{MG} and ΔT_{MG} respectively are the composition range at T_{mono} and the height of the miscibility gap; Δx_I and Δx_{II}, respectively denote the composition ranges of regions I and II at T_{mono} and ΔT_I and ΔT_{II} respectively denote the heights of regions I and II from T_{mono}. Cook and Hilliard [22] described a simple method to estimate the spinodal curve by using miscibility data. Although there are some limitations to this approach, they showed that the size of the spinodal is proportional to that of miscibility gap ($\Delta x_{MG} \approx \sqrt{3}\ \Delta x_{spinodal}$). Δx_I and Δx_{II} are determined by the spinodal line and the miscibility gap; therefore, they increase as Δx_{MG} increases. For the present systems, Δx_I and Δx_{II} are ~10 and 30 mol% of Δx_{MG}, respectively. Therefore, their sum becomes ~40 mol%, which agrees well with the result of Cook and Hilliard (42 mol%) [22]. On the other hand, ΔT_I and ΔT_{II} are determined from T_{mo} and the maximum and the minimum of the metastable liquidus; T_{mo} is known from the phase diagrams. However, since the maximum and the minimum of the metastable liquidus should be calculated from the phase relations between the liquid and solid phases, no simple expressions for ΔT_I and ΔT_{II} relative to the height of the miscibility gap can be derived [14]. As an analysis on the shape of metastable liquidus, Fig. 7 shows ΔT_I and ΔT_{II} as a function of slope of stable liquidus at T_{mo}. As the slope of

Table 2
Survey of experimental and calculated miscibility gap data in the rare earth silicate systems (in mol% and °C)

System	Critical point				Monotectic					
	Experimental		Present calc.		Experimental			Present calc.		
	x_c	T_c	x_c	T_c	x_1	x_2	T_{mo}	x_1	x_2	T_{mo}
La_2O_3–SiO_2	7.6	2075 [6]	9.65	2073	2.3	23.0	1675 [6]	1.3	22.3	1679
	6.0	2042 [9]								
Sm_2O_3–SiO_2	8.1	2190 [7]	11.9	2190	2.2	24.2	1700 [7]	0.8	23.3	1695
Dy_2O_3–SiO_2	8.0	2320 [8]	7.9	2319	1.3	22.0	1675 [8]	1.2	22.0	1681
Er_2O_3–SiO_2	11.4	2259 [8]	11.4	2263	1.4	22.7	1700 [8]	0.9	22.3	1690

Table 3
Sizes of miscibility gap, region I, and region II, and slopes at x_{mo} (in mol%, °C, and °C/mol%)

System	Δx_{MG}	Δx_I	Δx_{II}	ΔT_{MG}	ΔT_I	ΔT_{II}	$-(\text{slope})_I$	$-(\text{slope})_{II}$
La_2O_3–SiO_2	21.0	2.6	6.4	394	27	102	27.78	31.25
Sm_2O_3–SiO_2	22.5	2.1	6.4	495	30	157	31.33	50
Dy_2O_3–SiO_2	20.8	2.7	6.1	638	26	122	25	25
Er_2O_3–SiO_2	21.4	2.5	6.4	573	27	149	25	66.67

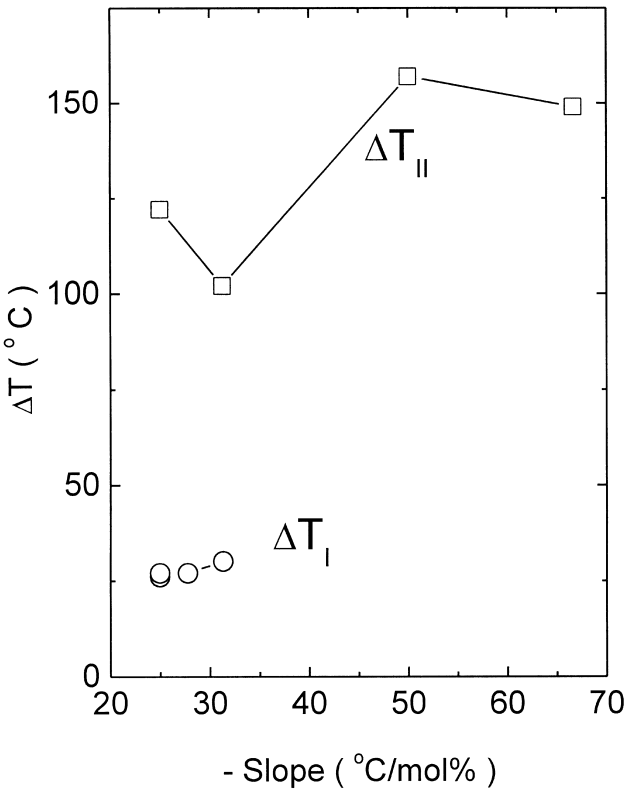

Fig. 7. Dependence of ΔT_{I} and ΔT_{II} on slopes at monotectic compositions in the rare earth silicate systems.

the stable liquidus increases, ΔT_{I} increases but ΔT_{II} does not increase simply in the present systems. This observation implies that the height of regions I and II is dependent on the size of miscibility gaps and the location of SiO_2. From the above discussion, it is found that the composition ranges of regions I and II can be predicted but the their heights cannot be estimated from the phase diagrams. Therefore, regions I and II cannot be obtained by simply extrapolating the stable liquidus near T_{mo}.

The boundaries of regions I and II consist of monotectic temperature, spinodal, and metastable liquidus. According to Cahn's suggestion [10], the location of the metastable liquidus can be easily approximated, because it is only an extrapolation of the stable liquidus. However, as discussed in the previous paper [14], no quantitative relation for the heights of regions I and II exists between the stable miscibility gap and the metastable liquidus. Therefore, it is very difficult to obtain a reasonable metastable liquidus inside the stable miscibility gap. Furthermore, obtaining the metastable liquidus surfaces in higher component systems by extending the liquidus surfaces is unlikely. It is desirable to use the analytical expression for the Gibbs free energy of the liquid phase to find the exact metastable liquidus. Because the thermodynamic modeling method always works, irrespective of the length of the stable liquidus, it must be applied to obtain the reasonable regions I and II, especially in case of the short stable liquidus, such as those in rare-earth silicate systems.

4. Conclusions

A thermodynamic modeling of phase diagrams in the binary La_2O_3–SiO_2, Sm_2O_3–SiO_2, Dy_2O_3–SiO_2, and Er_2O_3–SiO_2 systems was described by using the Gibbs free energies of the phases. The subregular solution model was applied to describe the liquid phases in these systems. The interaction parameters in the excess-Gibbs-free-energy expression of liquid phases were obtained by using the miscibility data through the multiple-linear-regression method. The present calculated miscibility gaps agreed well with the experimental data that were available in the literature. By calculating the metastable liquidus, the regions where a metastable solid can exist were obtained. Also, the possible composition range where liquid–liquid phase separation can occur via a spinodal decomposition process was calculated.

References

[1] W.A. Weyl, Coloured Glasses, 2nd Edition, Society of Glass Technology, Sheffield, UK, 1976.
[2] J.T. Kohli, Faraday effect in lanthanide-doped oxide glasses, in: B.G. Potter Jr., A.J. Bruce (Eds.), Synthesis and Application of Lanthanide-Doped Materials, The American Ceramic Society, USA, 1996, pp. 125–136.
[3] J. Fu, J. Am. Ceram. Soc. 83 (2000) 1004.
[4] J.E. Shelby, Key Eng. Mater. 94/95 (1994) 1.
[5] J.E. Shelby, Key Eng. Mater. 94/95 (1994) 345.
[6] N.A. Toropov, I.A. Bondar, Izv. Akad. Nauk SSSR, Otd. Khim. Nauk 8 (1961) 739.
[7] N.A. Toropov, I.A. Bondar, Izv. Akad. Nauk SSSR, Otd. Khim. Nauk 8 (1961) 1372.
[8] N.A. Toropov, F.Ya. Galakhov, S.F. Konovalova, Izv. Akad. Nauk SSSR, Otd. Khim. Nauk 8 (1961) 1365.
[9] V.B.M. Hageman, H.A.J. Oonk, Phys. Chem. Glasses 27 (1986) 194.
[10] J.W. Cahn, J. Am. Ceram. Soc. 52 (1969) 118.
[11] L. Li, Z. Tang, W. Sun, P. Wang, Phys. Chem. Glasses 38 (1997) 323.
[12] L. Li, Z. Tang, W. Sun, P. Wang, Phys. Chem. Glasses 40 (1999) 126.
[13] O. Redlich, A.T. Kister, Ind. Eng. Chem. 40 (1948) 345.
[14] S.S. Kim, T.H. Sanders Jr., J. Am. Ceram. Soc. 82 (1999) 1901.
[15] J. Vrestal, J. Velisek, CALPHAD 6 (1982) 297.
[16] F.C. Kracek, J. Am. Chem. Soc. 52 (1930) 1436.
[17] G.V. Samsonov (Ed.), The Oxide Handbook, 2nd Edition, IFI/PLENUM, New York, Washington DC, and London, UK, 1982.
[18] P. Wu, A.D. Pelton, J. Alloy Comp. 179 (1992) 259.
[19] S.S. Kim, T.H. Sanders Jr., J. Am. Ceram. Soc. 74 (1991) 1833.
[20] A. Dietzel, Z. Elektrochem. 48 (1942) 9.
[21] E.M. Levin, J. Am. Ceram. Soc. 50 (1967) 29.
[22] H.E. Cook, J.E. Hilliard, Trans. Met. Soc. AIME 233 (1965) 142.